Journal of Molecular Structure 1247 (2022) 131344

Contents lists available at ScienceDirect

Journal of Molecular Structure

journal homepage: www.elsevier.com/locate/molstr

Design and synthesis of 1,4-disubstituted 1,2,3-triazoles: Biological evaluation, *in silico* molecular docking and ADME screening

İrfan Şahin[a], Mustafa Çeşme[a], Fatma Betül Özgeriş[b], Özge Güngör[a], Ferhan Tümer[a,*]

[a] Department of Chemistry, Faculty of Art and Sciences, Kahramanmaras Sutcu Imam University, 46040, Kahramanmaras, Turkey
[b] Department of Nutrition and Dietetics, Faculty of Health Sciences, Ataturk University, Erzurum, Turkey

ARTICLE INFO

Article history:
Received 5 July 2021
Revised 17 August 2021
Accepted 18 August 2021
Available online 24 August 2021

Keywords:
Triazoles
Anticancer
Antioxidant activity
α-Amylase inhibition
Molecular docking
ADME

ABSTRACT

In this study, propargyl compounds were synthesized from 4-hydroxybenzaldehyde and 3–methoxy-4-hydroxybenzaldehyde (**2a-2b**). As a result of click reactions of synthesized propargyl compounds (**2a-b**) with organic azides (**4a-4e**), carbonyl compounds (**5a-5 h**) having 1,2,3-triazole skeleton were obtained. The structures of the synthesized compounds were illuminated by FTIR, $^{1}H/^{13}C$ NMR spectroscopies and elemental analyses. Antioxidant and anti-cancer and α-amylase enzyme inhibition studies of the synthesized compounds were carried out, and the effects of different functional groups in the compounds on the activity were investigated. When the results of the α-amylase enzyme inhibition studies of the synthesized compounds were compared with the reference drug acarbose (IC_{50}: 891 µg/mL), it was determined that all compounds (IC_{50}: 165–1471 µg/mL) showed higher activity than acarbose, except for compounds **5a** and **5c**. In particular, compound **5 g** (IC_{50}: 165 µg/mL) was found to have approximately 5.5 times higher activity than acarbose. When the DPPH• radical scavenging studies were examined, all compounds showed a higher activity than the standard BHT and β-carotene. According to $ABTS^{\bullet+}$ radical scavenging activity results, all compounds showed more effective activity than Ascorbic acid, and Trolox used as standard. Compound **5a** showed approximately the same scavenging effect with β-carotene and BHT. Compounds were also screened for anti-cancer activities against the HeLa cell line. According to the results, **5c** (IC_{50}: 50.12 µg/mL) and **5 h** (IC_{50}: 57.07 µg/mL) exhibit moderate antitumor activity compared to *cis*-platin against the HeLa cell line. The molecules have been studied in detail for their ADME properties and have not violated any drug-likeness rules. In addition, they exhibited a high oral bioavailability profile, as their BBB (Blood Brain Barrier) penetration and GI (gastrointestinal) absorption properties were favorable. Molecular docking results show that all compounds have a high affinity for the active site of α-amylase.

1. Introduction

Despite remarkable technological advances in diagnosing and treating diseases in recent years, cancer is one of the chiefly causes of death worldwide [1,2]. This disease damages different organs and occurs at various tissue levels. Although outstanding progress has been made in cancer treatment, ineffective chemotherapy caused by drug resistance, and many drug's inabilities to distinguish between cancerous cells and normal cells, research studies of agents with fewer side effects continue intensively [3,4].

Heterocyclic compounds are ringed compounds containing one or more heteroatoms. The most common heteroatoms are nitrogen, oxygen, and sulfur, but studies of new compounds containing them are quite large and continue to increase daily. Heterocyclic compounds are spread over an extensive area in nature and are essential for life [5]. They play a crucial role in the metabolism of all living cells. Examples of heterocyclic compounds are purine and pyrimidine bases of DNA, essential amino acids (proline, histidine, tryptophan), several vitamins and coenzyme precursors (thiamine, riboflavin, pyridoxine, folic acid, biotin, vitamin B12 and E families), photosynthesizing pigment. In addition, chlorophyll, oxygen-carrying pigment (hemoglobin), many hormones (kinetin, serotonin, histamine) and most sugars can be given [6–9]. Heterocyclics with nitrogen atoms in their structure are of great importance in the pharmaceutical industry and organic chemistry [10,11]. In five-member ring systems, structures with three nitrogen atoms are defined as triazoles. Triazole refers to one of a pair of isomeric chemical compounds with the closed formula $C_2H_3N_3$. These com-

* Corresponding author at: Department of Chemistry, Faculty of Art and Sciences, Kahramanmaras Sutcu Imam University, 46040, Kahramanmaras, Turkey.
E-mail addresses: mustafacesme@msn.com (M. Çeşme), betul.ozgeris@atauni.edu.tr (F.B. Özgeriş), ftumer@ksu.edu.tr (F. Tümer).

https://doi.org/10.1016/j.molstruc.2021.131344
0022-2860/

Fig. 1. Structures of 1,2,3-triazole and 1,2,4-triazole.

pounds are of two types, 1,2,3-triazoles and 1,2,4-triazoles [12,13]. (Fig. 1.)

Molecules with a 1,2,3-Triazole skeleton are highly preferred in medicinal chemistry. They can be easily bound to biomolecular targets as they show high stability even in robust oxidative and reductive environments, increasing their resolution of the tendency to perform hydrogen bonding, dipole-dipole and π stacking interactions. In addition, compounds containing 1,2,3- triazole group are compounds with various biological activities (anticancer, antimicrobial, anti-tubercular, anticonvulsant, antibacterial, anti-inflammatory, analgesic, antiviral, and anti-HIV agents) that are extremely important [13].

Organic compounds with an aldehyde group in their structure are found in combined or non –combined forms in many plants in nature and function significantly as an intermediate. Aldehydes have effective antimicrobial properties and are typically used for high-level disinfection in health care environments [14–16]. It is also used in agriculture for the preparation of herbicides and plant growth regulators [17,18].

Oxygen is an essential element for life [19]. When cells use oxygen to produce energy, free radicals form ATP production (adenosine triphosphate) by the mitochondria [20]. Free radical molecules are unstable and highly reactive molecules containing unpaired electrons [21]. Free radicals can damage the nucleus, DNA, proteins, carbohydrates and many biological molecules such as lipids [22]. They also cause cell damage. Free radicals are usually removed or inactivated by antioxidants in vivo environments [23,24].

In this work, we report the design and synthesis of various 1,2,3-triazole compounds (**5a-h**) with aldehyde groups. Structures of the compounds were characterized by FTIR, $^{1}H/^{13}C$ NMR and elemental analyses. Then antioxidant, anti-cancer and α-amylase enzyme activity studies were investigated. Finally, computational parameters like molecular docking study and ADME prediction of synthesized compounds were performed.

2. Materials and methods

2.1. Materials and instrumentation

All reagents and solvents were of reagent-grade quality and obtained from commercial suppliers (Aldrich or Merck) and used as received unless noted otherwise. Elemental analyses (C, H, N) were performed using a Costech ECS 4010 (CHN). Infrared spectra were recorded on a Perkin-Elmer FT-IR spectrometer (Spectrum 400) kitted with an ATR apparatus. 1H/13C NMR spectra were recorded on a Bruker 400 MHz instrument, and TMS was used as an internal standard. The 1H/13C NMR spectra of the compounds were investigated in CDCl3 solvent. α-Amylase enzyme inhibition activity determined by Hitachi U3900H Spectrophotometer.

2.2. Synthesis method of compounds (5a-h)

All compounds were obtained according to our previous work [25]. $^{1}H/^{13}C$ NMR, FT-IR spectra of the compounds are given in the supplementary. The general synthesis procedure was depicted in Scheme 1.

3–methoxy-4-(prop–2-yn-1-yloxy)benzaldehyde (2b): m.p.: 80–81 °C. **Yield**: 87%. **color**: Dark yellow solid. **FTIR** (υ, cm^{-1}): 3249, 2985 (C–H), 2823 (-O-CH_2), 2114 (-C≡CH), 1691 (-HC=O), 1589, 1512, 1468, 1426, 1379, 1269, 1221, 1168, 1123, 1008. **^{1}H NMR** (400 MHz, $CDCl_3$) δ 9.89 (s, 1H), 7.48 (dd, J = 8.2, 1.8 Hz, 1H), 7.45 (d, J = 1.8 Hz, 1H), 7.16 (d, J = 8.2 Hz, 1H), 4.87 (d, J = 2.4 Hz, 2H), 3.96 (s, 3H), 2.58 (t, J = 2.4 Hz, 1H). **^{13}C NMR** (100 MHz, $CDCl_3$) δ 190.84, 152.15, 150.10, 131.00, 126.20, 112.70, 109.58, 77.49, 76.64, 56.64, 56.05.

1-azido-4-methoxybenzene (4a): Yield: 87%, Colour: Brown Oily. FTIR (υ, cm^{-1}): 3003 (C–H), 2836, 2105 (-N_3), 1609, 1465.

1-azido-4-isopropylbenzene (4b): Yield: 93%. color: Dark Brown oily. FTIR (υ, cm^{-1}): 2962 (C–H), 2871, 2096 (-N_3), 1605, 1461.

1-azido-4-methylbenzene (4c): Yield: 90%. color: Dark Brown oily. FTIR (υ, cm^{-1}): 3029 (C–H), 2864, 2097 (-N_3), 1613, 1581, 1503, 1452.

1-azido-4-chlorobenzene (4d): Yield: 97%. color: Light Brown oily. FTIR (υ, cm^{-1}): 3472, 3381 (C–H), 2091 (-N_3), 1614, 1485.

1-azido-4-fluorobenzene (4e): Yield: 83%. color: Dark Brown oily. FTIR (υ, cm^{-1}): 3229 (C–H), 2986, 2108 (-N_3), 1737, 1598, 1498.

4-((1-(p-tolyl)–1H-1,2,3-triazol-4-yl)methoxy)benzaldehyde (5a): m.p.: 128–129 °C. **color**: Cream solid. **Yield**: 87%. **FTIR** (υ, cm^{-1}): 3163 (C–H), 2839–2756 (C–H), 1682 (C=O), 1602–1508 (C=C), 1427 (*N = N*), 1302 (C–N), 1242 (C–O), 814 (=C–H). **^{1}H NMR**: (400 MHz, $CDCl_3$) δ 9.91 (s, 1H), 8.07 (s, 1H), 7.87 (d, J = 8.5 Hz, 2H), 7.62 (d, J = 8.3 Hz, 2H), 7.34 (d, J = 8.4 Hz, 2H), 7.16 (d, J = 8.6 Hz, 2H), 5.39 (s, 2H), 2.44 (s, 3H). **^{13}C NMR**: (100 MHz, $CDCl_3$) δ 190.74, 163.12, 143.91, 139.24, 134.61, 132.04, 130.47, 130.32, 121.24, 120.55, 115.13, 62.18, 21.10. **Anal. calcd. for $C_{17}H_{15}N_3O_2$**: C, 69.61; H, 5.15; N, 14.33. Found: C, 68.13; H, 5.36; N, 14.09.

4-((1-(4-chlorophenyl)–1H-1,2,3-triazol-4-yl)methoxy)benzaldehyde (5b): **m.p.**: 143–144 °C. **color**: Light yellow solid. **Yield**: 94%. **FTIR** (υ, cm^{-1}): 3151, 3081 (C–H), 2842–2758 (C–H), 1686 (C=O), 1601–1500 (C=C), 1442 (*N = N*), 1302 (C–N), 1243–1228 (C–O), 819 (=C–H). **^{1}H NMR**: (400 MHz, $CDCl_3$) δ 9.91 (s, 1H), 8.23 (s, 1H), 7.87 (d, J = 8.2 Hz, 2H), 7.73 (d, J = 8.7 Hz, 2H), 7.52 (d, J = 8.6 Hz, 2H), 7.16 (d, J = 8.5 Hz, 2H), 5.38 (s, 2H). **^{13}C NMR**: (100 MHz, $CDCl_3$) δ 190.73, 163.00, 134.87, 132.06, 130.53, 130.09, 121.86, 115.10, 61.99. **Anal. calcd. for $C_{16}H_{12}ClN_3O_2$:** C, 61.25; H, 3.86; N, 13.39. Found: C, 61.25; H, 3.83; N, 13.01.

4-((1-(4-fluorophenyl)–1H-1,2,3-triazol-4-yl)methoxy)benzaldehyde (5c): **m.p.**: 134–135 °C. **color**: Dark yellow solid. **Yield**: 92%. **FTIR** (υ, cm^{-1}): 3155–3074 (C–H), 2837–2755 (C–H), 1686 (C=O), 1601–1575 (C=C), 1421 (*N = N*), 1302 (C–N), 1255- 1225 (C–O), 814 (=C–H). **^{1}H NMR**: (400 MHz, $CDCl_3$) δ 9.90 (s, 1H), 8.14 (s, 1H), 7.87 (d, J = 8.5 Hz, 2H), 7.78 – 7.71 (m, 2H), 7.23 (t, J = 12.6 Hz, 2H), 7.15 (d, J = 8.6 Hz, 2H), 5.38 (s, 2H). **^{13}C NMR**: (100 MHz, $CDCl_3$) δ 190.73, 163.82, 163.03, 161.33, 132.04, 130.50, 122.73, 122.65, 116.97, 116.74, 115.10, 62.04. **Anal. calcd. for $C_{16}H_{12}FN_3O_2$:** C, 64.64; H, 4.07; N, 14.13. Found: C, 62.58; H, 4.52; N, 13.93.

3–methoxy-4-((1-(4-methoxyphenyl)–1H-1,2,3-triazol-4-yl)methoxy)benzaldehyde (5d): **m.p.**: 111–112 °C. **color**: Light Brown solid. **Yield**: 89%. **FTIR** (υ, cm^{-1}): 3080 (C–H), 2947–2832 (C–H), 1677 (C=O), 1512 (C=C), 1471 (*N = N*), 1306 (C–N), 1257-1221 (C–O), 830 (=C–H). **^{1}H NMR**: (400 MHz, $CDCl_3$) δ 9.87 (s, 1H), 8.13 (s, 1H), 7.63 (d, J = 8.9 Hz, 2H), 7.46 (d, J = 7.9 Hz, 1H), 7.44 (s, 1H), 7.29 (d, J = 7.9 Hz, 1H), 7.02 (d, J = 8.8 Hz, 2H), 5.46 (s, 2H), 3.94 (s, 3H), 3.87 (s, 3H). **^{13}C NMR**: (100 MHz, $CDCl_3$) δ 190.88, 160.01, 153.02, 149.97, 130.69, 126.71, 122.31, 114.86, 112.59, 109.31, 62.83, 56.04, 55.63. **Anal. calcd. for $C_{18}H_{17}N_3O_4$**: C, 63.71; H, 5.05; N, 12.38. Found: C, 63.42; H, 5.06; N, 11.98.

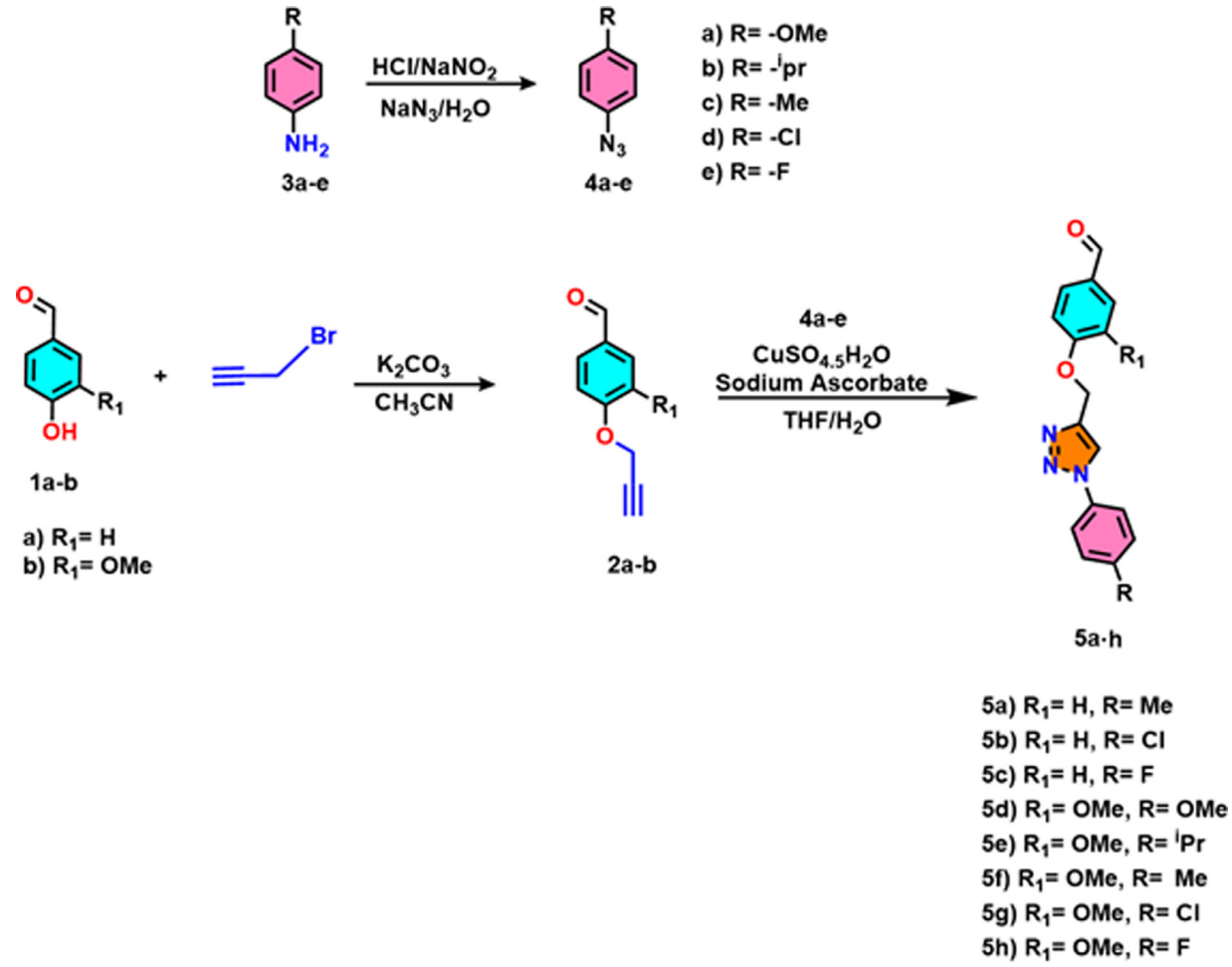

Scheme 1. Synthetic route for compounds (**5a-h**).

4-((1-(4-isopropylphenyl)−1H-1,2,3-triazol-4-yl)methoxy)−3-methoxybenzaldehyde (5e): **m.p.**: 95–96 °C. **color**: Powder solid. **Yield**: 86%. **FTIR** (υ, cm^{-1}): 3139, 3102 (C–H), 2960- 2834 (C–H), 1685–1672 (C=O), 1585- 1508 (C=C), 1461 (*N = N*), 1347 (C–N), 1263 (C–O), 833 (=C–H). **^{1}H NMR**: (400 MHz, $CDCl_3$) δ 9.88 (s, 1H), 8.23 (s, 1H), 7.66 (d, J = 8.4 Hz, 2H), 7.47 (d, J = 10.7 Hz, 2H), 7.39 (d, J = 8.2 Hz, 2H), 7.31 (s, 1H), 5.48 (s, 2H), 3.96 (s, 3H), 3.05 – 2.95 (m, 1H), 1.30 (d, J = 6.9 Hz, 6H). **^{13}C NMR**: (100 MHz, $CDCl_3$) δ 190.90, 153.00, 150.13, 149.99, 135.16, 130.72, 127.80, 126.76, 120.79, 112.62, 109.29, 62.79, 56.06, 33.85, 23.86. **Anal. calcd. for $C_{20}H_{21}N_3O_3$**: C, 68.36; H, 6.02; N, 11.96. Found: C, 69.24; H, 5.99; N, 11.35.

3–methoxy-4-((1-(p-tolyl)−1H-1,2,3-triazol-4-yl)methoxy)benzaldehyde (5f): **m.p.**: 118–119 °C. **color**: Dark red solid. **Yield**: 83%. **FTIR** (υ, cm^{-1}): 3151, 3077 (C–H), 2913–2853 (C–H), 1682 (C=O), 1598–1586 (C=C), 1470 (*N = N*), 1344 (C–N), 1280- 1221 (C–O), 801 (=C–H). **^{1}H NMR**: (400 MHz, $CDCl_3$) δ 9.88 (s, 1H), 8.11 (s, 1H), 7.61 (d, J = 8.3 Hz, 2H), 7.48 (s, 1H), 7.46 (d, J = 3.7 Hz, 1H), 7.33 (d, J = 8.2 Hz, 2H), 7.29 (d, J = 6.5 Hz, 1H), 5.48 (s, 2H), 3.96 (s, 3H), 2.44 (s, 3H). **^{13}C NMR**: (100 MHz, $CDCl_3$) δ 190.96, 152.99, 149.93, 139.19, 134.67, 134.64, 130.66, 130.32, 126.80, 120.55, 112.52, 109.22, 62.88, 56.05, 21.12. **Anal. calcd. for $C_{18}H_{17}N_3O_3$**: C, 66.86; H, 5.30; N, 13.00. Found: C, 66.38; H, 5.32; N, 12.06.

4-((1-(4-chlorophenyl)−1H-1,2,3-triazol-4-yl)methoxy)−3-methoxybenzaldehyde (5 g): **m.p.**: 120–121 °C. **color**: Yellow solid. **Yield**: 93%. **FTIR** (υ, cm^{-1}): 3137, 3076 (C–H), 3004- 2942 (C–H), 1690 (C=O), 1588 (C=C), 1464 (*N = N*), 1346 (C–N), 1262-1222 (C–O), 804 (=C–H). **^{1}H NMR**: (400 MHz, $CDCl_3$) δ 9.89 (s, 1H), 8.13 (s, 1H), 7.71 (d, J = 8.9 Hz, 2H), 7.53 (d, J = 8.9 Hz, 2H), 7.50 – 7.45 (m, 2H), 7.27 (s, 1H), 5.49 (s, 2H), 3.97 (s, 3H). **^{13}C NMR**: (100 MHz, $CDCl_3$) δ 190.90, 152.87, 149.94, 144.29, 135.34, 134.87, 130.77, 130.03, 126.72, 121.78, 121.29, 112.49, 109.29, 62.79, 56.06. **Anal. calcd. for $C_{17}H_{14}ClN_3O_3$**: C, 59.40; H, 4.11; N, 12.22. Found: C, 61.21; H, 4.02; N, 11.37.

4-((1-(4-fluorophenyl)−1H-1,2,3-triazol-4-yl)methoxy)−3-methoxybenzaldehyde (5 h): **m.p.**: 113–114 °C. **color**: Cream solid. **Yield**: 67%. **FTIR** (υ, cm^{-1}): 3155, 3099 (C–H), 3007–2959 (C–H), 1685 (C=O), 1584 (C=C), 1424 (*N = N*), 1262- 1236 (C–O), 831(=C–H). **^{1}H NMR**: (400 MHz, $CDCl_3$) δ 9.87 (s, 1H), 8.15 (s, 1H), 7.77 – 7.68 (m, 2H), 7.49 – 7.43 (m, 2H), 7.27 – 7.19 (m, 3H), 5.47 (s, 2H), 3.95 (s, 3H). **^{13}C NMR**: (100 MHz, $CDCl_3$) δ 190.88, 163.80, 161.32, 152.91, 149.95, 133.30, 130.76, 126.68, 122.72, 122.63, 116.95, 116.71, 112.54, 109.34, 62.75, 56.04. **Anal. calcd. for $C_{17}H_{14}FN_3O_3$**: C, 62.38; H, 4.31; N, 12.84. Found: C, 63.37; H, 4.40; N, 12.34.

2.3. Biological assays

2.3.1. Evaluation of antioxidant activity

The total radical scavenging capacity of the tested compounds was determined by the DPPH• scavenging method as per the reported procedure compared to that of BHT, β-Carotene, Trolox and ascorbic acid [26]. The solution of DPPH• was daily prepared, stored in a flask coated with aluminum foil and kept in the dark at 4 °C. In brief, a fresh solution of DPPH• (0.1 mM) was prepared

in ethanol. Then, 1.5 mL of each compound in ethanol was added an aliquot (0.5 mL) of this solution (6.25 – 200 µg/mL). These mixtures were mixed firmly and incubated in the dark for 30 min. Finally, the absorbance value was logged at 517 nm in a spectrophotometer [27].

$ABTS^{\bullet+}$ scavenging method is based on the ability of the method described by *Re* et al. [26]. The ABTS solution (2 mM) in water with the oxidizing agent of potassium persulfate (2.3 mM) yielded the ABTS cation radical ($ABTS^{\bullet+}$), which was soluble in both aqueous and organic solvents. It was diluted with phosphate buffer (0.1 mM, pH 7.4) to adjust inquired absorbance (0.700 ± 0.025) at 734 nm. Finally, tested samples solution (3 mL) at various concentrations (6.25–200 µg/mL) has interacted with $ABTS^{\bullet+}$ (1 mL) and the remaining absorbance was spectrophotometrically recorded at 734 nm.

The capability to scavenge the DPPH• and $ABTS^{\bullet+}$ radical was calculated using the following equation (Eq. 1).

$$RSE\ (\%) = \left[1 - \frac{Asample}{Acontrol}\right] \times 100 \quad (1)$$

where RSE is radical scavenging effects, AC is the absorbance value of the control and AS is the absorbance value of the sample [28].

The half-maximal scavenging concentration of the sample (IC_{50}) was determined from the graph plotted inhibition percentage against all compounds concentrations (µg/mL) [29].

Cupric ions (Cu^{2+}) reducing power was used as the reducing ability method for compounds **5a-h**. Cu^{2+} reducing capability was performed according to the reported method [30]. For this purpose, aliquots of $CuCl_2$ solution (0.25 mL, 0.01 M), ethanolic neocuproine solution (0.25 mL, 7.5×10^{-3} M), and NH_4Ac buffer solution (0.25 mL, 1 M) were transferred to a test tube, which contains compounds **5a-h** at different concentrations (6.25–200 µg/mL). Total volume was completed with distilled H_2O to 2 mL and shaken. The absorbance of samples was recorded at 450 nm after 30 min.

2.3.2. Preparation of Hela cells culture

The human cervix Hela cell line was purchased from ATCC (American Type Culture Collection, Manassas, VA, USA). The cells were grown and maintained in Dulbecco's Modified Eagle Medium/Nutrient Mixture F-12 (DMEM-F12) medium containing 10% fetal bovine serum (FBS) and 1% penicillin-streptomycin (Gibco, Life Technologies GmbH, Germany). Cells were cultured in a humidified atmosphere at 37 °C in 5% CO_2. The medium was refreshed every two days.

2.3.3. Measurement of cell growth by MTT assay

Anti-proliferative effects of **5a-h** on Hela were determined by MTT cell proliferation assay. MTT (3-[4,5-*dimethylthiazol*-2-*yl*]−2,5-diphenyltetrazolium bromide) is a yellow auxiliary agent that reduced formazan crystals in living cells. MTT was purchased from Sigma Chemical Company (St. Louis, Missouri, USA). 2×10^4 cells were inoculated in each well of 96- well plates. The cells were incubated in the absence or presence of **5a-h** (6.25,12.5, 25, 50, 100, 200, 400,800 µg/ml) for 48 h. After incubation periods, 20 µl of MTT solution (MTT stock solution: 5 mg/ml in phosphate-buffered saline) was added to each well, and the cells were incubated at 37 °C, 5% CO_2 containing incubator for 3 h. Then, plates were centrifuged at 1800 rpm for 10 min. The supernatant was removed, and 150 µl DMSO (Sigma-Aldrich®, USA) was added to each well to dissolve the formazan crystals. Finally, the absorbance values were measured at 570 nm by a spectrophotometer [31]. The viability was determined as the percentage of absorbance of **5a-h** treated cultures compared with untreated control cultures. In the experiment, cells treated with 1% Triton X-100 (Sigma-Aldrich®) were used as the positive control, while cells not treated with **5a-h** were used as the negative control [31].

2.3.4. α-Amylase enzyme inhibition activity

The stock solution of α-amylase enzyme purchased from Sigma Aldrich was prepared in DMSO solvent with a concentration of 10 mg/10 mL. Reagent solution was used as control, and enzyme activity was checked at different concentrations (50, 100, 200 µg/mL) without test sample. Starch solution (0.5%) was prepared by stirring and boiling starch (0.5 g) in deionized water (100 mL) for 15 min. To prepare the enzyme solution, 100 mg of the enzyme solution (1 unit/mL) was taken and mixed with 100 mL of 20 mM sodium phosphate buffer (pH 6.9). The color reagent was prepared by mixing 2 M NaOH (8 mL), deionized water (12 mL) and 96 mM 3,5-dinitrosalicylic acid (DNSA). Acarbose (1 mg/mL) was used as reference. Test solution (25 µL) and enzyme solution (50 µL) were mixed in vials and incubated for half an hour at 25 °C. Starch solution (50 µL) was added after incubation. It was then incubated for another 15 min. Color reagent (100 µL) was added to the mixture, and the mixture was heated in a water bath at 85 °C for 15 min. The reaction mixture was then cooled by removing it from the water bath, and absorbance values at 540 nm were recorded. Measurements were made triplicate for each sample. The control experiment was performed by replacing the drug sample (25 µL) with DMSO [32]. Inhibition values were calculated using the following equation: (Eq. 2).

$$\%\ Inhibition = \left(Acontrol - \frac{Aexample}{Acontrol}\right) \times 100 \quad (2)$$

2.3.5. Statistical analysis

Statistical analysis was performed using SPSS Statistics for Windows, statistical program SPSS software (version 20.0, SPSS, Chicago, IL, USA. Duncan's test was used to determine whether any treatment significantly differed from controls or each other. Statistical decisions were made with a significance level of 0.05.

2.4. Cheminformatics studies

The compound's physicochemical and pharmacological properties were calculated using the Molinspiration cheminformatics online software [33] (Molinspiration Cheminformatics, SK 90,026 Slovensky Grob, SR) and swissADME [34] web tool to monitor the compounds against the Lipinski RO5. Chemical structures and smiles notations of the synthetic compounds were obtained by BIOVIA Draw 2019 software. The smiles notations of compounds were then fed in Molinspiration and swissADME to calculate many molecular and ADME properties. Absorption (% ABS) of compounds from the intestine was assessed by the following formula:

$$\%\ ABS = 109 \times (0.345 \times TPSA)$$

2.5. Molecular docking studies

2.5.1. Ligand preparation for docking

In this study, 3D structures for synthesized compounds were sketched in drawing BIOVIA Draw 2019 software. All the compound's 3D structures were energy minimized using the MM2 minimization algorithm by Chem3D 20. All the minimized structures were converted into PDB or SDF file format before carrying out molecular docking analysis. Molecular electrostatic potential map calculations of compounds have been performed by utilizing Schrödinger Maestro Release 2021–1 [35].

2.5.2. Receptor preparation for docking

The X-ray crystal structure protein, the Human pancreatic alpha-amylase complexed with nitrite and acarbose (PDB code:

2QV4, 1.97 Å), was retrieved from the RCSB protein data bank PDB' (http://www.rcsb.org/pdb). Water molecules, ions, heteroatoms, and other ligands existing in the protein target were removed using Discovery Studio 2020 software. The downloaded structure of the protein target was converted into PDB format for molecular docking analysis.

2.5.3. Molecular docking process

In silico docking studies, compounds were docked against the 2QV4, and the docking scoring function was conducted using PyRx docking (academic licensed version 0.9.8) software. In this analysis, flexible-ligand:rigid-receptor docking was performed, and accurate docking conditions were selected [36]. The interactions were analyzed for the docking of ligands into active protein sites and estimating the binding affinities of docked compounds. For the generation of the grid, studies were executed using the PyRx Autodock Vina wizard. The grid on the ligand-binding site of the protein 2QV4 was centered at the binding site of X:12.385, Y:48.136, Z:26.209, and the grid dimensions size were 25×25×25 $Å^3$ dimensions with 0.375 Å. The exhaustiveness value of the protein has been set at 8. Nine poses were estimated for each ligand/compound with the protein. The binding energies of nine docked conformations of each ligand against the protein have been recorded for further assessment and visualization. The results of the best docking poses of the interactions were visualized and analyzed using Discovery Studio 2020. The obtained scoring function (binding energies (kcal/mol)) gives a score based on the best-docked ligand complex is picked out. The more negative the binding energy results from the interaction, the more stable the small molecule and the complex formed by the protein [36].

3. Results and discussion

3.1. Chemistry

This study aimed to change the substituents in two different regions of 1,2,3-triazole molecules containing aldehyde groups. The -H and -OMe groups have been changed in the aryl ring at position 4, where it is in the aldehyde group relative to the triazole ring. On the ring at position 1 -OMe, -^{i}Pr, Me, -Cl and -F groups have been changed and the effect of the groups on the molecule has been investigated.

This study aims to determine the effects of 1,2,3 triazole compounds on antioxidant, anti-cancer, ADME, molecular docking, according to functional groups. Azides (**4a-e**), propargyl compounds (**2a-b**) and 1,2,3-triazole compounds (**5a-h**) were synthesized in high yields concerning our previous study [25]. All compounds except compound **5e** and **5 h** were synthesized previously by Rao et al. [37] and Bistrovic et al. [38] (Table S2). The melting points, ^{1}H/^{13}C NMR spectra of the compounds agree with the literature value. The synthesized compounds structures were described by elemental analysis, FT-IR, ^{1}H/^{13}C NMR (Scheme 1).

3.2. Structural characterization analysis of the compounds

Spectroscopic data of all synthesized triazole compounds are given in the experimental section. FTIR spectra of all compounds are given in **Fig. S1-S14**. The characteristic vibrational bands of the N_3 group in azide compounds and the alkyne group in propargyl compounds were observed around ν 2100 cm^{-1}. These bands vanish as a result of the "click reaction" of azide and propargyl compounds. The vibrational band of the characteristic aldehyde group (HC=*O*) in propargyl and triazole compounds are detected as a sharp peak around ν 1685 cm^{-1}. The presence of characteristic bands in the FT-IR spectra of the compounds confirms their structure.

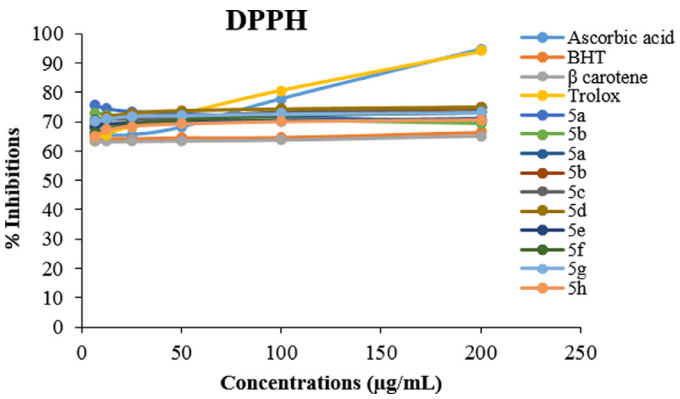

Fig. 2. DPPH free radical scavenging activity of different concentrations (6.25-200 µg/mL) of compound **5a-h** and reference antioxidants; Trolox, BHT, β-Carotene and ascorbic acid.

^{1}H/^{13}C NMR spectra of compounds were investigated, and the resulting spectral data were given in the experimental section and spectra were provided in supplementary documents (**Fig. S15-S32**). The ^{1}H/^{13}C NMR signals of the triazole and phenyl rings are similar in all compounds and the spectra of compound **5e** were discussed as representative. In the ^{1}H NMR spectrum of **5e** (**Fig. S25**), the methyl protons in the isopropyl group resonated as a doublet at δ 1.30 ppm. Again, the -CH- proton in the isopropyl group resonated as heptet at δ 3.00 ppm. The methoxy group in the benzaldehyde ring is singlet at δ 3.96 ppm, and the signal of etheric methylene protons (–OCH_2-) is singlet at δ 5.48 ppm. Singlet signal at δ 7.31 ppm and doublet at δ 7.47 (J = 10.7 Hz) ppm belong to the 3 protons in the aldehyde substituted benzene ring. The doublets observed at δ 7.39 (J = 8.2 Hz) and δ 7.66 (J = 8.4 Hz) ppm are signals of protons in the isopropyl substituted benzene ring. The -CH- proton in the triazole ring resonated as a singlet at δ 8.23 ppm. The singlet observed at δ 9.88 ppm belongs to the aldehyde proton. In the ^{13}C NMR spectrum of **5e** (**Fig. S25**), the signals of methyl carbon (2 x -CH_3) atoms belong to the isopropyl group are seen at δ 23.86 ppm. The signal observed at δ 33.85 ppm is the resonance signal of the -CH- carbon atom in the isopropyl group. The carbon atom signal of the methoxy group in the benzaldehyde ring was observed at δ 56.06 ppm, and the signal belonging to the carbon atom (O–CH_2) at the place where the triazole ring was attached to oxygen was observed at δ 62.79 ppm. At δ 120.79 ppm, the signal for the -C-H carbon in the triazole ring was observed [39,40]. The signals of the aromatic carbon atoms and the carbon atom in the triazole ring are observed in the range of δ 109.29–153.0 ppm. The carbonyl carbon of the aldehyde (-C=O) group was observed at δ 190.90 ppm.

3.3. Antioxidant activity

Antioxidant properties, especially radical scavenging activities, are significant due to removing the harmful effects of free radicals in biological systems. DPPH$^•$ and ABTS$^{•+}$ have been widely used to analyze the free radical scavenging efficacy of various antioxidant substances [41]. In this study, the antioxidant activity of the newly synthesized compounds **5a-h** and standard antioxidants such as Trolox, BHT, β-Carotene and Ascorbic acid were determined using DPPH$^•$ and ABTS$^{•+}$ methods. The samples were examined for their radical scavenging capabilities ranging between 6.25-200 µg/mL concentrations. Fig. 2 defines a significant decrease (P<0.05) in the concentration of DPPH$^•$ radical due to the scavenging ability of compounds and standards.

The scavenging effect of compounds **5a-h** and standards on the DPPH$^•$ radical decreased in the order of **Ascorbic acid > Trolox >**

Table 1
Determination of half-maximal concentrations (IC_{50}, μg/mL) of compounds **5a-h** and standards for DPPH• and ABTS•+ scavenging.

Compounds	DPPH• scavenging IC_{50} (μg/mL)	ABTS•+ scavenging IC_{50} (μg/mL)
Ascorbic acid	3.05±0.001	35.15±0.007
Trolox	6.76±0.002	19.20±0.004
BHT	10.73±0.001	4.82±0.001
β-Carotene	9.74±0.003	4.78±0.002
5a	8.91±0.004	4.99±0.005
5b	8.92±0.002	5.98±0.001
5c	9.11±0.001	5.93±0.003
5d	9.31±0.002	5.96±0.004
5e	9.15±0.005	5.99±0.002
5f	9.48±0.001	6.01±0.001
5g	8.94±0.003	5.81±0.002
5h	9.59±0.002	5.91±0.003

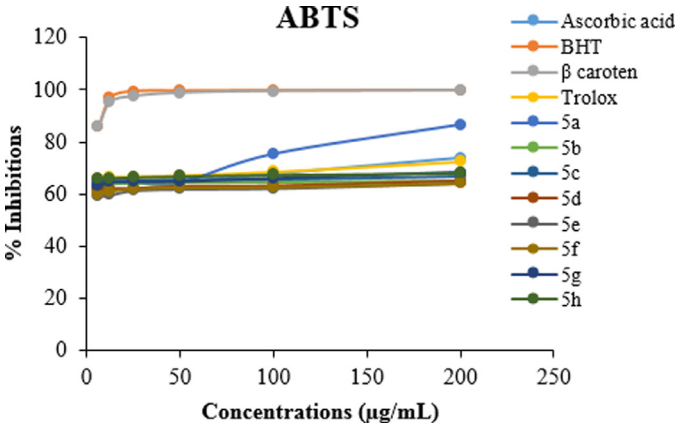

Fig. 3. ABTS radical scavenging activity of different concentrations (6.25–200 μg/mL) of compound **5a-h** and reference antioxidants; Trolox, BHT, β-Carotene and ascorbic acid.

5a > 5b > 5d > 5 *g* > 5c > 5e > 5f > 5 *h* > BHT > β-Carotene which were 94.95%, 94.41%, 70.63%, 70.12%, 70.06%, 69.87%, 68.55%, 68.55%, 65.92%, 65.17%, 64.96%, 63.23% at the concentration of 200 μg/mL, respectively. Free radical scavenging activity of these samples also increased with an increasing concentration.

IC_{50} values of DPPH• radical scavenging are as shown as Table 1. A lower IC_{50} value indicates a higher DPPH• free radical scavenging effect (Table 1). The DPPH• activity of **5a-h** are higher than **BHT** and **β-Carotene** standards.

All tested compounds exhibited effective radical scavenging activity against ABTS•+ radicals (p>0.001). As seen in Fig. 3, all compounds had effective ABTS+ radical scavenging activity in a concentration dependent manner (6.25 - 200 μg/mL). The scavenging effect of compounds and standards on the ABTS•+ radicals decreased in the order of BHT > β-Carotene > 5a > 5 *g* > 5 *h* > 5c > 5d > 5b > 5e > 5f > Ascorbic acid > Trolox, which were 99.31%, 99.17%, 86.62%, 68.31%, 67.97%, 66.75%, 64.93%, 64.91%, 63.98%, 63.98%, 35.47%, 31.99% at the concentration of 200 μg/mL, respectively. Free radical scavenging activity of these samples also increased with an increasing concentration.

IC_{50} values for compounds 5a-h and standards are shown Table 1. As with the DPPH• method, a lower IC_{50} value indicates a higher ABTS•+ radical scavenging ability. All compounds showed better ABTS•+ radical scavenging ability than Ascorbic acid and Trolox standards. Especially compound 5a has almost the same activity as BHT and β-Carotene.

The values of the CUPRAC method, in which the chromogenic neocuproine was used as the oxidizing agent, are shown in Table 2. The highest CUPRAC value was observed in the ascorbic acid. The compound **5e** showed higher activity than β-Carotene. At the same concentration (200 μg/mL), reducing capacities decreased in the order of **Ascorbic acid > Trolox > BHT > 5e > β-Carotene > 5d > 5a > 5 *h* > 5b > 5 *g* > 5f > 5c.**

Table 2
Determination of reducing power of same concentration (200 μg/mL) of compounds and standards by cupric ions (Cu^{2+}) reducing capacity by Cuprac method.

Antioxidants	Cu^{2+}- Cu^{+} reducing λ_{450}*
Trolox	0.1735 ± 0.002
BHT	0.1512 ± 0.001
β-Carotene	0.0875 ± 0.001
Ascorbic acid	0.9605 ± 0.002
5a	0.0738 ± 0.001
5b	0.0667 ± 0.002
5c	0.0626 ± 0.001
5d	0.0823 ± 0.004
5e	0.0925 ± 0.002
5f	0.0634 ± 0.004
5 g	0.0632 ± 0.003
5h	0.0687 ± 0.005

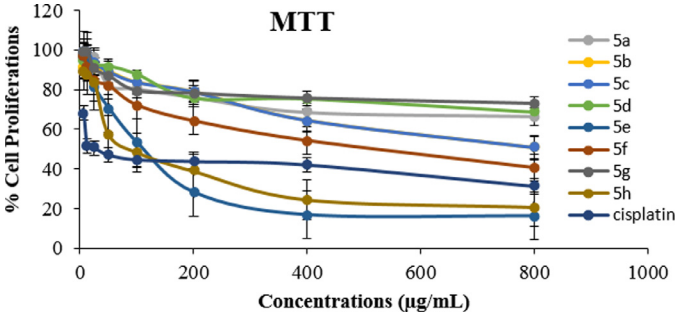

Fig. 4. Cytotoxic effects of **5a-h** on Hela cells (p < 0.05) (Error bars represents standard deviations (SD), p < 0.05 was considered as significant).

Table 3
Anti-cancer activity of the compounds against the HeLa cell line.

Comp.	MTT IC_{50} (μg/mL)
5a	77.73±0.003
5b	75.02±0.005
5c	50.12±0.002
5d	129.12±0.003
5e	112.71±0.002
5f	1394.12±0.001
5 g	181.87±0.004
5h	57.07±0.005
***Cis*-platin**	16.30±0.003

3.4. Anti-cancer activity

The synthesized compounds **5a-h** were screened for cytotoxic activity against the Hela cell line. Hela cells were treated with increasing concentrations of **5a-h** for 48 h, and MTT cell proliferation assays were carried out to determine the anti-proliferative effects of the agent on these cells [42]. The cells were exposed to compounds **5a-h** from 6.25 to 800 μg/ml. *Cis*-platin, one of the most effective anti-cancer agents, was used as the positive control. The results showed that there were dose-dependent decreases in cell proliferation compared to untreated controls (p < 0.05) (Fig. 4.) IC_{50} values for compounds **5a-h** were given in Table 3.

All compounds showed anti-cancer activity. The IC_{50} values of compounds **5a-h** are as follows, 77.73, 75.02, 50.12, 129.12, 112.71, 1394.12, 181.87, 57.07, respectively. Especially when the IC_{50}

Table 4
α-amylase inhibition IC_{50} values of synthesized compounds.

Comp.	IC_{50} (μg/mL)
5a	1471±0.003
5b	840±0.008
5c	1391±0.006
5d	315±0.005
5e	239±0.001
5f	248±0.003
5 g	165±0.005
5h	248±0.001
Acarbose	891

values of **5c** and **5 h,** which have a fluorine group in 1-position aromatic ring, were examined, it was seen that they had moderate activity against Hela cell line compared to *cis*-platinum (IC_{50}: 16.30 μg/mL).

3.5. α-Amylase enzyme activity

α-Amylase enzyme inhibition is of great importance in the treatment of diabetes, as it delays glucose absorption. One way to reduce high sugar in the blood (hyperglycemia) is to delay the digestion of carbohydrates in the intestine through digestive enzyme inhibitors; it is envisaged as a new solution for the treatment of diabetes. Acarbose is used as an α-amylase inhibitor in the literature [43,44]. The α-amylase activity of the compounds synthesized in this study was determined using the 3,5-dinitrosalicylic acid (DNSA) method. Results were compared with acarbose used as standard (Table 4). The α-amylase inhibition IC_{50} values of the compounds are as follows, 1471, 840, 1391, 315, 239, 248, 165, 248 from **5a** to **5 h**, respectively. In general, compounds with a methoxy ($-OCH_3$) group on the aromatic ring at the 4-position (**5d-h**), showed higher inhibitory activity compared to the compounds without the methoxy group (**5a-c**). In particular, compound **5 g**, which has a methoxy ($-OCH_3$) group in the 4-position aromatic ring and a chlorine group in the 1-position aromatic ring, exhibited the highest activity. Also, compound **5 g** has about 5.5 times higher activity than the standard acarbose (IC_{50}: 891) [45].

3.6. In-silico adme results

ADME data improves the selection and identification at the therapeutic dose of molecules with an optimal safety profile, together with the drug discovery process, instead of the final phase. This assessment prevents waste of time and valuable resources on medication molecules that are disposable over time.

Also known as Pfizer's rule of five or merely the rule of five (RO5), Lipinski's five rules are a practical rule for assessing drug similarity or figuring out whether a chemical compound with a particular pharmacological or biological activity has favorable chemical properties and physical properties which would make it an orally active drug in humans. Christopher A. Lipinski formulated the rule [46] based on the observation that most orally administered drugs are relatively small to moderately lipophilic molecules. The rule describes the molecular properties essential to the human body's pharmacokinetics, including their absorption, distribution, metabolism, and excretion (ADME). The rule states that if a ligand molecule violates Lipinski's rule 5, it has more than 5 hydrogen bond donors, the molecular weight is above 500, the log P is above 5, and N and O atoms are more than 10. As a result, inadequate absorption or permeability is more likely for compounds and drug candidates. Drug likeness is a qualitative term about how a chemical compound or drug candidate molecule is "drug-like" regarding factors such as bioavailability used in drug design. With a more specific expression, a complex balance of different molecular properties and structural features that decide whether a specific molecule is comparable to known drugs can be described as drug similarity. These properties primarily influence any living organism's molecular behaviors, including hydrophobicity, electronic dispersion, hydrogen bonding properties, molecular size, flexibility, and the existence of different pharmacophoric properties, bioavailability, protein affinity, reactivity, toxicity, metabolic stability, and transport properties.

Molecular properties such as partition coefficient (Log Po/w), topological polar surface area (TPSA), hydrogen bond donors and acceptors, rotatable bonds, number of atoms, molecular weight, and violations of Lipinski's rule of five were calculated to assess the drug-likeness of the compounds and represented in Table 5.

The Lipinski rules recommend no more than one violation of an orally bioactive drug or drug candidate. ADME data showed that all values calculated for synthetic compounds fell within anticipated ranges as described in Lipinski's rule of five. All synthesized compounds fully complied with the Lipinski rules and did not exhibit any violations of these rules.

Bioavailability radar chart screened for compounds for prompt assessment of drug similarity. This radar chart illustrates six different physicochemical properties: lipophilicity, size, polarity, solubility, flexibility, and saturation. On each axis, a physicochemical range is depicted as a pink area, defined by default with identifiers adapted from SwissADME, which must fall on the radar plot of the molecule to be considered fully drug-like. Consistent with this model, all compounds exhibited a high oral bioavailability profile, as seen in the bioavailability radar charts (Fig. 5). On the other hand, if the topological polar surface area (TPSA) values are greater than 130 $Å^2$, the compound's oral bioavailability is considered low. The TPSA value is between 57.01 and 75.47 for all compounds.

The compounds BOILED-Egg diagram is shown in Fig. 6. The BOILED-Egg is the main feature of this diagram, which is an intuitive way for predicting two major ADME characteristics at the same time: passive gastrointestinal absorption (HIA) and brain access (BBB: Blood-Brain Barrier). Although this classification model is conceptually basic because it only uses two physicochemical descriptors (WLOGP and TPSA, for lipophilicity and apparent polarity, respectively), it was designed with great care in terms of statistical significance and robustness. BOILED-Egg diagram consists of gray and yellow area. Both compartments are not one another exclusive. The outside gray area stands for molecules with properties implying predicted low absorption and limited brain penetration. In practice, the BOILED-Egg diagram has proven straightforward interpretation and efficient translation to molecular design in various drug discovery studies [34]. We can conclude from the red dot position for our compounds that BBB penetration and GI absorption property are positive, and the PGP effect on the molecule is negative. All molecules are positioned within the range within the specified limits.

In order to elucidate the qualitative structure-activity relationships of synthetic compounds **(5a-h)**, physicochemical properties and calculations were carried out using molinspiration cheminformatics software. A molecule's lipophilic character be subject to two critical factors, i.e., hydrophobicity and polarity, which assist the molecule cross or irreversibly detriment the cellular membrane. The molecular lipophilicity potential (MLP) map and polar surface areas (PSAs) of synthetic compounds are given in Fig. S33.

In the present study, compounds 5a, 5b and 5c (PSA:57.01) were the most active, followed by compounds 5e, 5f, 5 g, 5 h and 5d with PSAs of 66.24, and 75.47, respectively. On the other hand, compounds 5a, 5b, and 5c showed similar PSAs, while compound 5e showed a greater lipophilic area than compounds 5b and 5 g. Similarly, although the PSA of compound 5d was higher than that

Table 5
Physicochemical and drug-likeliness properties of synthetic compounds (**5a-h**) according to the rule of five.

	MW	%Abs	TPSA(Å²)	RB	HBA	HBD	Log Po/w	LV	BS	SA	WS
Comp.	Rules										
	<500	>80	<130	≤ 9	≤ 10	≤ 5	≤ 5	≤ 1	–	–	–
5a	293.32	89.33	57.01	5	4	0	2.67	0	0.55	2.56	−3.53
5b	313.74	89.33	57.01	5	4	0	2.90	0	0.55	2.49	−3.80
5c	297.28	89.33	57.01	5	5	0	2.65	0	0.55	2.42	−3.25
5d	339.35	82.96	75.47	7	6	0	2.30	0	0.55	2.82	−3.40
5e	351.40	86.15	66.24	7	5	0	3.27	0	0.55	2.96	−4.48
5f	323.35	86.15	66.24	6	5	0	2.66	0	0.55	2.78	−3.69
5g	343.76	86.15	66.24	6	5	0	2.83	0	0.55	2.70	−3.96
5h	327.31	86.15	66.24	6	6	0	2.63	0	0.55	2.64	−3.50

Key: MW: Molecular weight (gr/mol),**%Abs**: Percentage of absorption, **TPSA:** Topological polar surface area, **RB:** number of rotatable bonds, **HBA:** number of hydrogen bond acceptors, **HBD:** number of hydrogen bond donors, **LV:** number of Lipinski rule of 5 violations, **Log Po/w** (iLOGP): Lipophilicity, **BS:** Bioavailability score, **SA:** Synthetic accessibility [From 1 (very easy) to 10 (very difficult)], **WS:** Water solubility, Log *S* (Insoluable < −10 < Poorly < −6 < Moderately < −4 < Soluable < −2 Very < 0 < Highly).

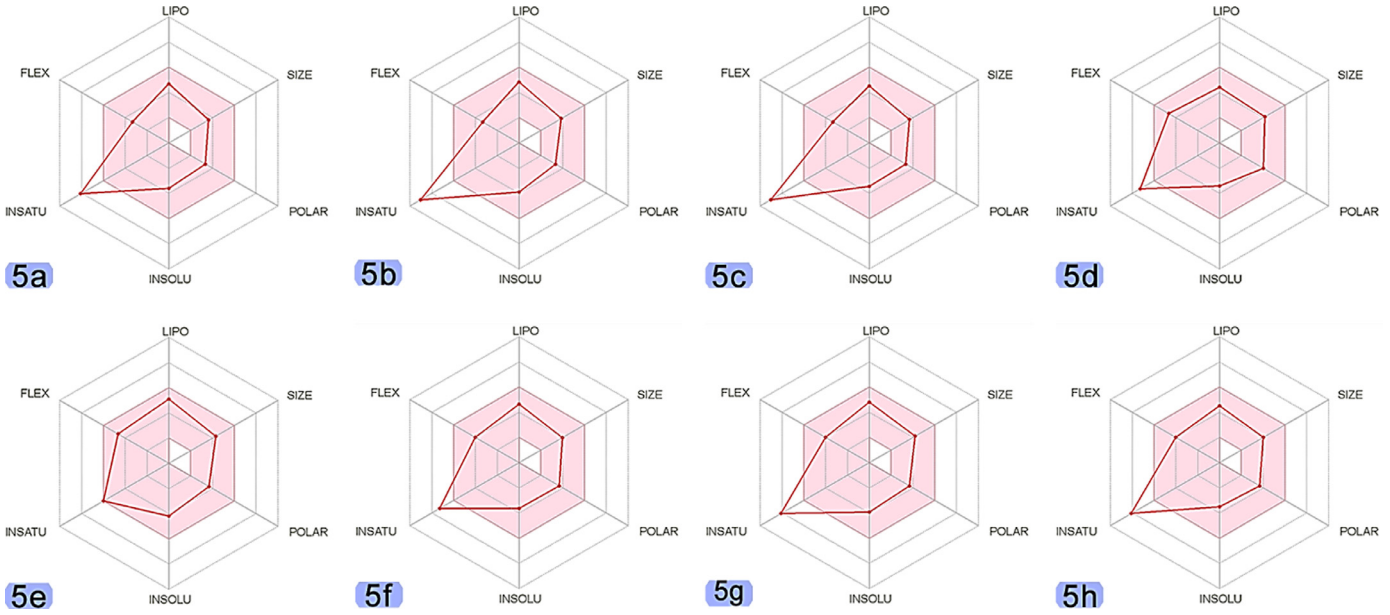

Fig. 5. Bioavailability radar related to physicochemical properties of molecules. The pink area symbolizes the ideal range for each properties (lipophilicity: (Criteria's: Lipophilicity: - 0.7 < XLOGP3 < ++5.0, Size: 150 MW 500 g/mol, Polarity: 20 < TPSA < 130 Å2, Insolubility: 0 < log *S* < 6, Insaturation, Flexibility: 0.25 < rotatable bonds < 9). POLAR (polarity), LIPO (lipophilicity), INSOLU (solubility), FLEX (flexibility), and INSATU (saturation).

of other compounds, their MLP maps were almost the same apart from compound 5e. In the light of the qualitative data obtained from PSA and MLP maps, it is possible to say that there is a common correlation between the structure-activity relationship, considering the biological activity tests performed. It is seen that these results also overlap with the data obtained from molecular docking studies.

3.7. Molecular electrostatic potential (MEP)

In such studies, it is essential to see the electrophilic and nucleophilic regions of the studied compounds before starting the molecular docking process to make a preliminary prediction and interpretation of which possible atoms or functional groups may interact with the relevant receptors. Calculation of the molecular electrostatic potential (MEP) plays an important role in drug research and development studies to verify the evidence for the reactivity of molecules as inhibitors [46,47]. Although MEP indicates the molecular size and shape of the positive, negative, and neutral electrostatic potential, these parameters can be an essential tool to predict and interpret the molecular structure of the investigated drugs and their physicochemically structure-activity and property relationships. Moreover, the MEP is a helpful tool for predicting drug reactivity to electrophilic and nucleophilic attacks [48-49]. The MEP of the total 8 compounds within the study's scope was calculated using the Adaptive Poisson-Boltzmann Solver (APBS) method and is given in Fig. 7. The maximum negative region in the MEP is the favored site for the electrophilic attack, as indicated by the red color. As a result, an attacking electrophile will be drawn to the negatively charged sites, while the blue regions will be saturated in the reverse direction [50]. Electrostatic potential increases are identified in the colors in red < orange < yellow < green < blue. Because the receptor and the corresponding ligands recognize each other at the molecular surfaces, the electrostatic potential value is mainly responsible for binding a substrate to the receptor binding sites. As a result, small red, yellow-orange, and blue patches on the larger green surface of compounds balance the hydrophilic and hydrophobic parts required for good quality protein-enzyme binding and interaction. The electrostatic potential scales of

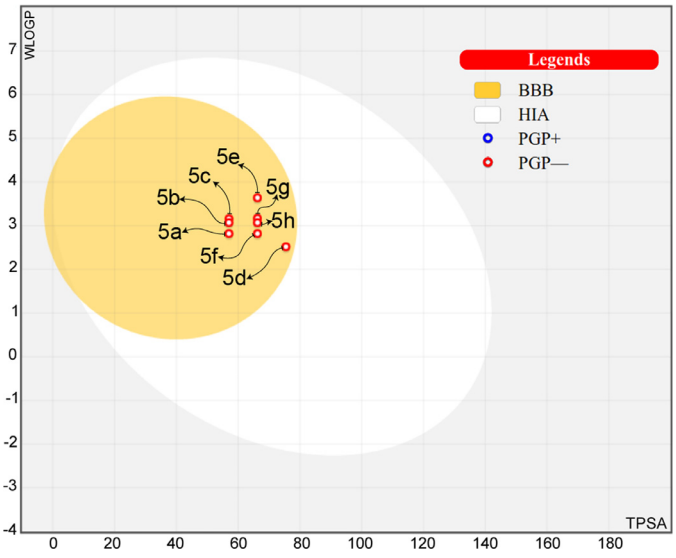

Fig. 6. The BOILED-Egg ADME diagram of the compounds (**5a-h**) WLOGP vs. TPSA. (Points located in the BOILED-Egg's yolk (yellow) signify the molecules predicted to passively permeate through the blood-brain barrier (BBB), whereas the ones in the egg white are relative to the molecules predicted to be passively absorbed by the gastrointestinal tract. The red ones point out to the molecules predicted not to be effluated from the CNS (Central Nervous System- by the P-glycoprotein). Yolk and white regions are not reciprocally exclusive.

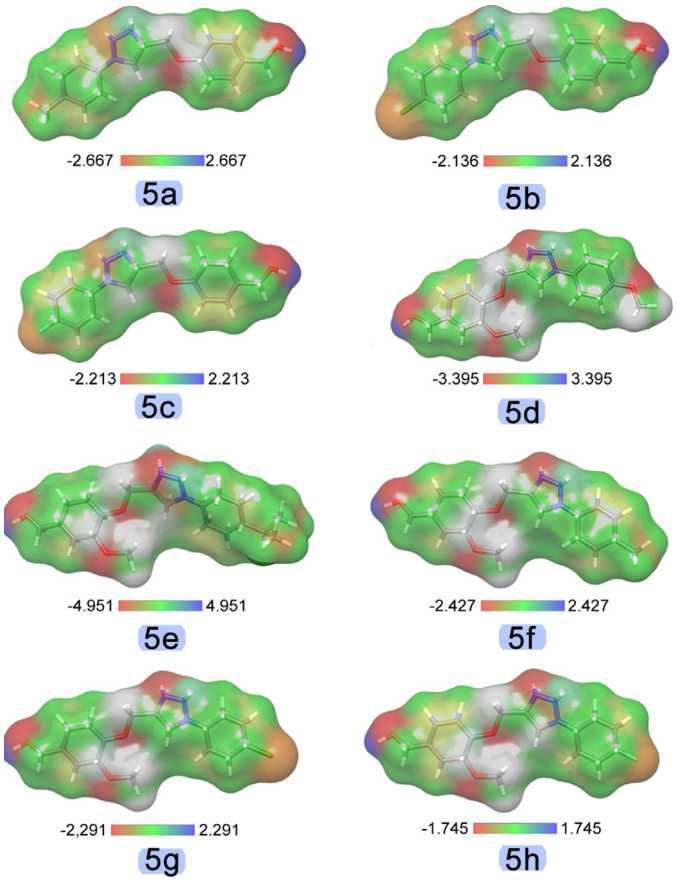

Fig. 7. The molecular electrostatic potential (MEP) surface of compounds.

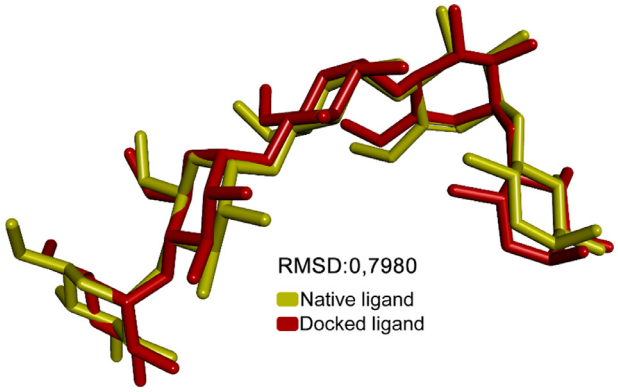

Fig. 8. Validation of molecular docking protocol.

5a-h compounds were calculated in the range between −4.951 and −4.951.

3.8. Molecular docking results

3.8.1. Validation of docking protocol

The molecular docking procedure was validated by assessing the binding poses of ligands in the protein-ligand complex crystal structure of the 2QV4 protein, which we used in the study. In the structure of Human pancreatic alpha-amylase (PDB ID: 2QV4), co-ligand acarbose (native ligand) is covalently linked to the receptor residues HIS-101, VAL-107, ALA-106, ASN-105, GLY-164, THR-163, HIS-299, TYR-62, ASP-300, ARG-195, GLU-233, GLN-63 and TRP-59. Therefore, in docking procedures, the amylase's receptor grid was selected by limiting it to the residues occupied by the acarbose ligand and interacting with the ligand area. For this process, the ligand (acarbose) in the X-ray crystal structure of the amylase enzyme was removed from the structure and re-docked to the protein's binding site. In the next step, the ligand's pose in the enzyme's crystal structure was compared with the pose obtained by redocking, and the mean square deviation (RMSD) value was calculated. According to the results, the co-crystallized ligand showed similar orientations and conformational poses as in the crystal structure when re-docked at the active binding sites of the target enzyme. The ligand in the crystal structure of amylase and the re-docked ligand were almost superimposed. We found that the RMSD value between crystal structure pose and re-docked acarbose pose in active α-amylase residues was 0.7980 Å (Fig. 8). Accordingly, since the calculated RMSD value was significantly lower than the maximum allowable value of 2.0 Å, it showed that the docking procedure performed in this study was valid.

3.8.2. Docking analysis results

The investigation of the binding interaction mechanisms of biomacromolecules with small molecules such as drugs or drug candidates has been caused a significant rise in molecular docking studies. In addition to being a powerful tool in rational drug design, molecular docking may predict the most stable structure and mode of interaction of receptor-ligand complex formation and allows for proper identification and investigation of interaction information during the production of new drugs [36].

This study investigated the affinity of 8 compounds we synthesized against human pancreatic α-amylase enzyme (HPA). The results of molecular docking on α-amylase are given in Table 6. The binding affinities obtained from the molecular docking results show that all compounds have a high affinity towards the active site of α-amylase. These values ranged from −8.9 to −8.2 kcal/mol for all compounds, with the highest binding affinity being −8.9 kcal/mol for compound 5a. In general, GLU233 and

Table 6
Interaction and amino acid residues involved in the inhibition of a-amylase enzyme summary.

Comp.	Binding affinity (kcal/mol)	Type of interaction bond	Involved receptor residues
5a	−8.9	HB, EC, HP	ALA198, GLN63, GLU233, TYR62, LYS200, ILE235, HIS201, TYR151, LEU162
5b	−8.7	HB,EC,HP	ALA198, HIS201, GLU233
5c	−8.7	HB, HP	GLN63, LEU165, ILE235, HIS201, LEU162, ALA198,
5d	−8.4	HB, EC, HP	GLN63, LYS200, GLU233, ASP197, ILE235, TYR62, HIS201, LEU165, TRP59, LEU162, ALA198
5e	−8.3	HB, EC, HP	HIS305, ASP197, GLU233, ASP300, ILE235, TRP59, LEU165, LEU162
5f	−8.4	HB, EC, HP	GLU233, ASP197, ASP300, ASP197, ILE235, HIS201, LYS200, TYR151, ALA198, LEU162
5g	−8.2	HB, HP	GLN63, THR163, LEU162, ILE235, HIS201, LYS200, ALA198, LEU165
5h	−8.6	HB, HL, HP	TRP59, ASP197, HIS299, ASP300, TYR62, LEU165

Key: HB:hydrogen bond; **C–HB**: Carbon-Hydrogen Bond, **EC**:electrostatic interaction, **HP**:hydrophobic interaction, **HL**:halogen bond.

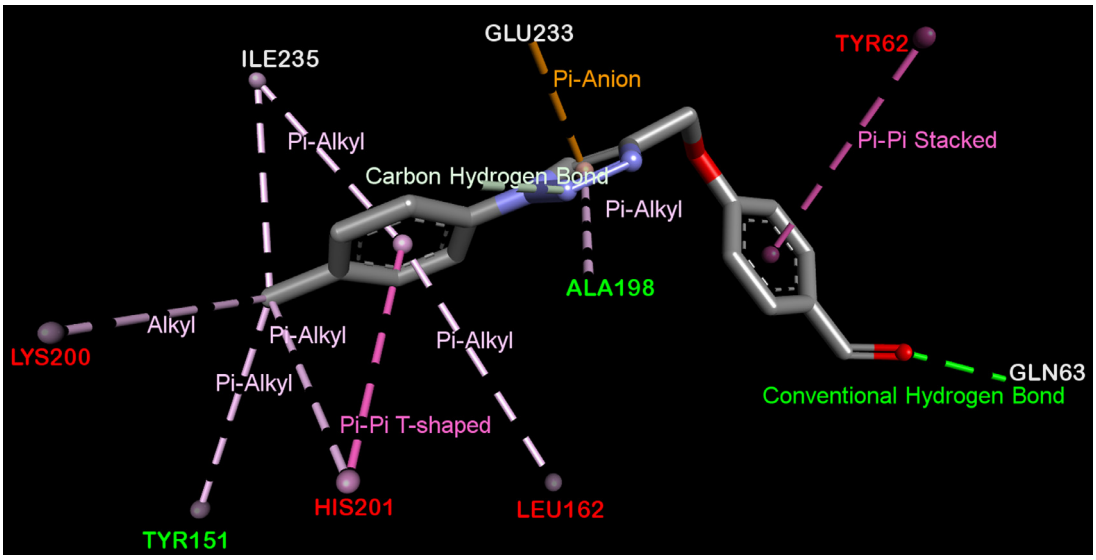

Fig. 9. 3D depiction of 5a compound which has maximum docking score with α-amylase.

ASP 300 residues play a role in the main interactions and bonds in all α-amylase-compounds (5a-h) complexes. These two residues are known to act as catalytic residues in the hydrolytic reactions of α-amylase [32]. The data showing the bonds, bond types, and bond lengths formed between the α-amylase and compounds are presented in detail, **Supporting Table 1**. For all molecules, predominantly hydrophobic interactions were responsible for anchoring at the active site of α-amylase in the formation of stable enzyme-compound complexes. This phenomenon can be explained by the predominance of hydrophobic bonding types in the complexation interaction with the active site of the α-amylase, as it will be associated with the low and moderate lipophilicity of the compounds, as can be seen from the lipophilicity potential of the molecules.

The 3D representation of the complex formed between 5a and α-amylase is given in Fig. 9, indicating the chemical bonding mode and bond types. This complex structure (5a- α-amylase) is formed between twelve different amino acid residues of α-amylase and **5a** atoms. It can be spotted from Fig. 9 that predominantly hydrophobic interactions are responsible for anchoring of compound **5a**. Nine different hydrophobic interactions occurred through Alkyl, Pi-Alkyl, Pi-Pi Stacked and Pi-Pi T-shaped bonding types. In the Pi-Alkyl binding modes, the direction of the interaction was formed from the compound **5a** to the ALA198, LEU162 and ILE235 residues via the Pi-Orbitals, while in TYR151 and HIS201 it was formed from the residues to **5a**. Similarly, **5a** formed Pi-interactions (Pi-Pi stacked, Pi-Pi T-shaped Pi-anion, and alkyl) with amino acid residues GLU233, TYR62, HIS201, ILE235, and LYS200. In addition, between the H bonds formed in the structure; While the conventional H bond was formed between GLN63 residue with the oxygen atom in the aldehyde group attached to the benzene ring in compound **5a**, C–H bond was formed over the second nitrogen atom in the triazole ring with the ALA 198 residue.

We noted that the interaction between the TRP 59 residue of the active site of **5b** and α-amylase in the **5b**-enzyme complex is hydrophobic interactions in the Pi-Pi Stacked (triazole moiety) and Pi-Alkyl (-Cl atom) type. In this strong interaction, we can see that ALA198 and HIS201 residues form a stable complex with the H-donor and H-acceptor over the oxygen atom in the aldehyde group attached to the benzene ring. Similarly, an electrostatic Pi-Anion interaction has occurred between the benzene ring to which the aldehyde group is attached and the GLU 233 residue. For the α-amylase-compound complexes, all the docked model illustrations are given in detail in Fig. 10.

When examining the results of molecular docking for compound **5c**, it is seen that the resulting complex is primarily due to hydrophobic interactions. Four different Pi-Alkyl bonds were formed from the hydrophobic interactions from **5c** to the residues LEU162 and ALA198 via the triazole and the benzene ring attached to this group. In addition, Pi-sigma interactions were established with ILE235 and LEU165 residues over the same benzene ring and the benzene ring attached to the aldehyde group, respectively. The occurrence of Pi-sigma interactions is generally thought to be due to hyperconjugation or bending (tilting) of the molecular structure.

In compound **5d,** the catalytic residue GLU233 formed a C–H bond interaction with the etheric methylene group attached to the triazole ring. In the triazole moiety of the compound, ASP197 formed an electrostatic interaction with the Pi-anion bond, and TYR62 formed a Pi-Pi stacked interaction. In the ring to which the aldehyde group is attached, the residues of LEU162, ALA198,

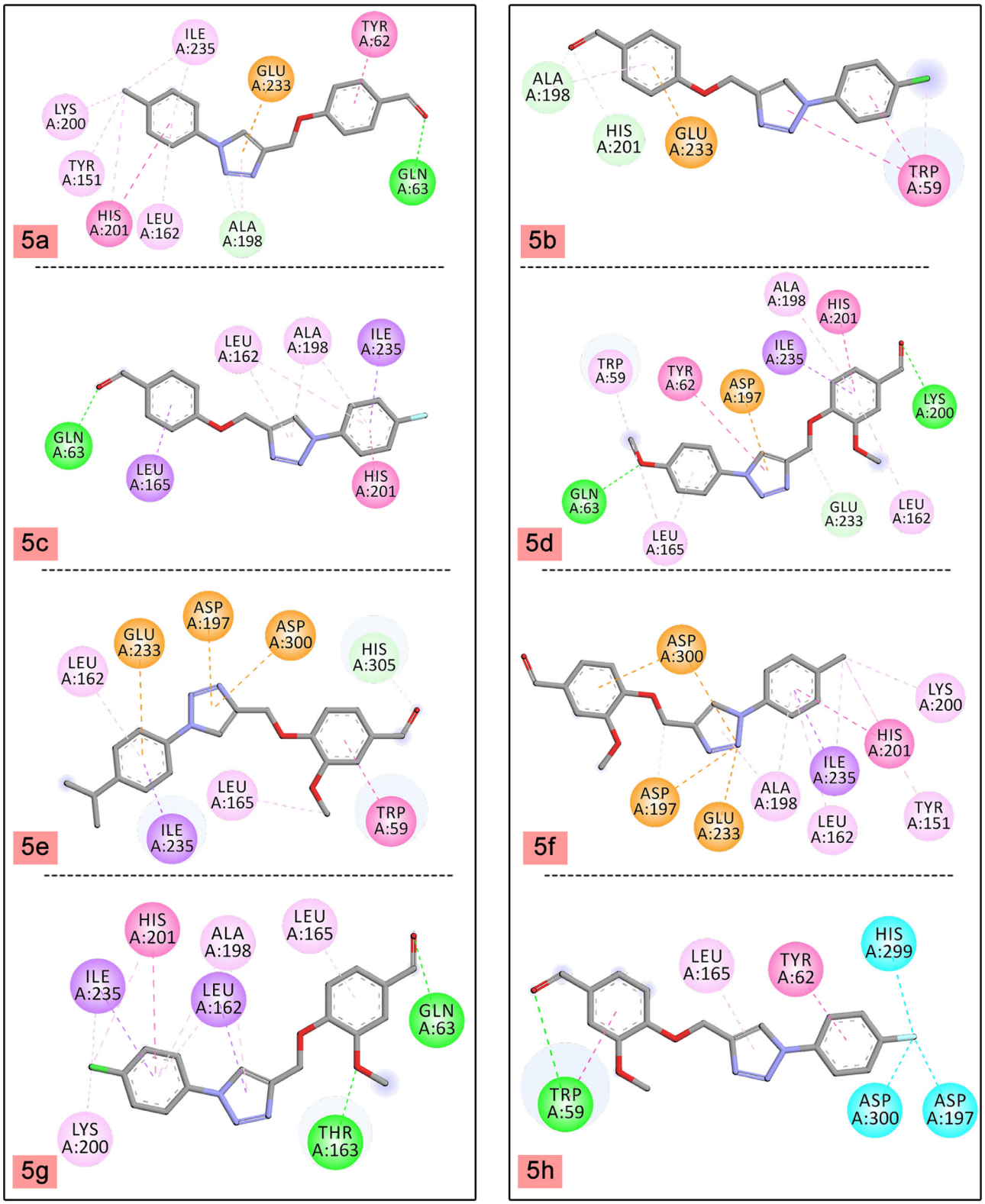

Fig. 10. 2D representations of the best pose interactions between the α-amylase and compounds.

HIS201, and ILE205 have interacted over the bonds Pi-Sigma, Pi-Pi Stacked, Pi-Pi T-shaped, Alkyl, Pi-Alkyl.

In addition to hydrophobic interactions in compound **5e**, electrostatic interactions came to the fore a little more. As in compound **5d**, the catalytic residue GLU233 exhibited an electrostatic interaction with the ring to which the methyl groups were attached via the Pi-Anion bond. The triazole ring is also electrostatically linked with residues ASP197 and ASP300 via the Pi-Anion bond. While HIS 305 interacted by forming an H bond over the aldehyde group oxygen, other moiety interactions of the molecule occurred through hydrophobic bonds (Pi-Sigma, Pi-Pi Stacked, Alkyl, and Pi-Alkyl) with residues ILE235, TRP59, LEU165, and LEU162.

Compound **5f** interacted with the catalytic residue GLU233 both by H bond and electrostatically forming a salt bridge. The salt bridge formed is due to the 1,3-dipolar structure of the triazole ring in which the nitrogen atom (middle one) has higher electron density resulting in dipole-dipole interactions with ALA198, GLU233, ASP197 and ASP300 residues. The other catalytic residue, ASP300, on the other hand, formed an electrostatically attractive charge interaction over the benzene ring in the aldehyde group and the positively charged nitrogen atom in the triazole moiety. While the residue ASP197 interacted with the etheric methylene group attached to the triazole ring via the C–H bond, it also interacted electrostatically with the nitrogen atom in the triazole ring. The methyl group has attached TYR151, TYR152, LEU162, ALA198, HIS201, and ILE235 in the ring to which the methyl group has formed hydrophobic interactions through the bonds Pi-Sigma, Pi-Pi Stacked, Pi-Pi T-shaped, Alkyl, and Pi-Alkyl.

When the complex structure formed for the **5 g** compound is examined; The residues in the active site of the enzyme showed a dominant binding tendency through the triazole moiety of the molecule, the benzene ring attached to this group, and the Cl atom in the ring. The resulting stable structure provided the Pi-Alkyl interaction with the residues ALA198, LEU165, LEU162 and ALA198 through the triazole region and the benzene ring attached to this group. The Cl atom is attached to the residues by hydrophobic Alkyl interaction with LYS200 and HIS201. While the GLN63 residue interacted by forming an H bond over the aldehyde group oxygen, the THR163 residue formed an H bond with the oxygen in the methoxy group in the same ring.

In compound **5 h**, unlike other compounds, Halogen interaction occurred through HIS299, ASP197 and the catalytic residue ASP300 over the fluorine atom in the structure. Interaction with the H bond was formed between the oxygen in the aldehyde group and the TRP59 residue. Two different Pi-Pi Stacked interactions were formed with the benzene ring of the **5 h** molecule with aldehyde and methoxy groups, the N atom in the indole structure of the TRP59 residue, and the benzene ring in the same structure.

4. Conclusion

In this paper, we synthesized and characterized 1,2,3-triazole based compounds *via* click chemistry and evaluated them for various biological activities. The synthesized compounds showed promising α-amylase, antioxidant and anti-cancer activity compared to related standard drugs. Compound **5 g** showed very high α-amylase inhibition activity compared to the standard drug acarbose. All compounds showed higher scavenging activity than β-carotene and BHT in DPPH• scavenging activity and higher scavenging activity than Ascorbic Acid and Trolox in $ABTS^{\bullet+}$ scavenging activity. Furthermore, compounds **5c** and **5 h** demonstrated moderate activity against the HeLa cell line compared to standard *cis*-platin. The molecules have been studied in detail for their ADME properties and have not violated any drug-likeness rules. In addition, they exhibited a high oral bioavailability profile, as their BBB (Blood Brain Barrier) penetration and GI (gastrointestinal) absorption properties were favorable. Furthermore, molecular docking study was performed to predict possible interaction modes and binding energies of the compounds for the active site of α-amylase.

Thus, suggesting that compounds from the present series **5a-h** can be further optimized and developed as lead molecules.

Declaration of Competing Interest

The authors declare no conflicts of interest.

CRediT authorship contribution statement

İrfan Şahin: Visualization, Investigation, Writing – review & editing. **Mustafa Çeşme:** Visualization, Investigation, Writing – review & editing. **Fatma Betül Özgeriş:** Visualization, Investigation, Writing – original draft. **Özge Güngör:** Visualization, Investigation. **Ferhan Tümer:** Supervision, Project administration, Methodology, Writing – review & editing.

Acknowledgments

The authors thanks Kahramanmaraş Sütçü İmam University Scientific Research Projects Unit (*Project code: BAP-2019/3–20 M*) (Turkey) for funding. Furthermore, we would like to thank the Higher Education Council Research Board (YÖK 100/2000 PhD. Scholarship Priority Areas Program "Molecular Pharmacology and Drug Research") for granting the Scholarship (to İrfan Şahin).

Supplementary materials

Supplementary material associated with this article can be found, in the online version, at doi:10.1016/j.molstruc.2021.131344.

References

[1] J.M. Cassady, W.M. Baird, C.J. Chang, Natural products as a source of potential cancer chemotherapeutic and chemopreventive agents1, J. Nat. Prod. 53 (1990) 23–41, doi:10.1021/np50067a003.
[2] K.D. Miller, R.L. Siegel, C.C. Lin, A.B. Mariotto, J.L. Kramer, J.H. Rowland, K.D. Stein, R. Alteri, A. Jemal, Cancer treatment and survivorship statistics, 2016, CA, Cancer J. Clin 66 (2016) 271–289, doi:10.3322/caac.21349.
[3] M. Gholampour, S. Ranjbar, N. Edraki, M. Mohabbati, O. Firuzi, M. Khoshneviszadeh, Click chemistry-assisted synthesis of novel aminonaphthoquinone-1,2,3-triazole hybrids and investigation of their cytotoxicity and cancer cell cycle alterations, Bioorg. Chem. 88 (2019) 102967.
[4] S.B. Pinki Yadav, Kashmiri Lal, Ashwani Kumar, Santosh Kumar Guru, Sundeep Jaglan, European journal of medicinal chemistry green synthesis and anticancer potential of chalcone linked-1, 2, 3- triazoles, Eur. J. Med. Chem. 126 (2017) 944–953, doi:10.1016/j.ejmech.2016.11.030.
[5] R. Neama, N.M. Aljamali, M. Jari, Synthesis, identification of heterocyclic compounds and study of biological activity, Asian J. Res. Chem. 7 (2014) 664–676.
[6] I. Ali, M.N. Lone, Z.A. Alothman, A. Alwarthan, Insights into the pharmacology of new heterocycles embedded with oxopyrrolidine rings: DNA binding, molecular docking, and anticancer studies, J. Mol. Liq. 234 (2017) 391–402.
[7] R. Dahm, Discovering DNA: friedrich Miescher and the early years of nucleic acid research, Hum. Genet. 122 (2008) 565–581, doi:10.1007/s00439-007-0433-0.
[8] H. McNab, A John, in: Joule and Keith Mills Heterocyclic Chemistry, 5th edn, Wiley-Blackwell, 2010, p. 640, doi:10.1002/aoc.1719. (paperback) ISBN 978-1-4051-3300-5, 2011.
[9] S. Rachwal, A.R. Katritzky, in: 1,2,3-Triazoles, in: Compr. Heterocycl. Chem. III, Elsevier, 2008, pp. 1–158, doi:10.1016/B978-008044992-0.00501-0.
[10] A. Deiters, S.F. Martin, Synthesis of oxygen- and nitrogen-containing heterocycles by ring-closing metathesis, Chem. Rev. 104 (2004) 2199–2238.
[11] A. Dhakshinamoorthy, H. Garcia, Metal-organic frameworks as solid catalysts for the synthesis of nitrogen-containing heterocycles, Chem. Soc. Rev. 43 (2014) 5750–5765, doi:10.1039/c3cs60442j.
[12] N. Sahu, J.K. Sahu, A. Kaushik, A Review on "Triazoles": their chemistry and pharmacological potentials, Curr. Res. Pharm. Sci. 03 (2013) 108–113.
[13] S. Rani, K. Raheja, V. Luxami, K. Paul, A review on diverse heterocyclic compounds as the privileged scaffolds in non-steroidal aromatase inhibitors, Bioorg. Chem. 113 (2021) 105017, doi:10.1016/j.bioorg.2021.105017.
[14] J. Skelley, Open source tactics: bargaining power for strategic litigation, J. Intellect. Prop. 16 (2016) 1–35.

[15] W.A. Rutala, D.J. Weber, New disinfection and sterilization methods, Emerg. Infect. Dis. 7 (2001) 348–353, doi:10.3201/eid0702.010241.
[16] S.E. Walsh, J.Y. Maillard, A.D. Russell, C.E. Catrenich, D.L. Charbonneau, R.G. Bartolo, Development of bacterial resistance to several biocides and effects on antibiotic susceptibility, J. Hosp. Infect. 55 (2003) 98–107, doi:10.1016/S0195-6701(03)00240-8.
[17] S.A. Güngör, M. Tümer, M. Köse, S. Erkan, Benzaldehyde derivatives with functional propargyl groups as α-glucosidase inhibitors, J. Mol. Struct. 1206 (2020) 127780, doi:10.1016/j.molstruc.2020.127780.
[18] L. Zhu, X. Xu, F. Zheng, Synthesis of benzaldehyde by swern oxidation of benzyl alcohol in a continuous flow microreactor system, Turkish J. Chem. 42 (2018) 75–85, doi:10.3906/kim-1704-42.
[19] B. Halliwell, J.M.C. Gutteridge, Free Radicals in Biology and Medicine, 3rd ed., Oxford University Press Inc., 2015, doi:10.1093/acprof:oso/9780198717478.001.0001.
[20] P. Abrescia, P. Golino, Free radicals and antioxidants in cardiovascular diseases, Expert Rev. Cardiovasc. Ther. 3 (2005) 159–171, doi:10.1586/14779072.3.1.159.
[21] M. Valko, M. Izakovic, M. Mazur, C.J. Rhodes, J. Telser, Role of oxygen radicals in DNA damage and cancer incidence, Mol. Cell. Biochem. 266 (2004) 37–56, doi:10.1023/B:MCBI.0000049134.69131.89.
[22] M. Valko, D. Leibfritz, J. Moncol, M.T.D. Cronin, M. Mazur, J. Telser, Free radicals and antioxidants in normal physiological functions and human disease, Int. J. Biochem. Cell Biol. 39 (2007) 44–84, doi:10.1016/j.biocel.2006.07.001.
[23] W. Droge, Free radicals in the physiological control of cell function, Physiol. Rev. 82 (2002) 47–95.
[24] J.K. Willcox, S.L. Ash, G.L. Catignani, Antioxidants and prevention of chronic disease, Crit. Rev. Food Sci. Nutr. 44 (2004) 275–295, doi:10.1080/10408690490468489.
[25] İ. Şahin, F.B. Özgeriş, M. Köse, E. Bakan, F. Tümer, Synthesis, characterization, and antioxidant and anticancer activity of 1,4-Disubstituted 1,2,3-triazoles, J. Mol. Struct. 1232 (2021) 130042, doi:10.1016/j.molstruc.2021.130042.
[26] R. RE, Antioxidant Activity Applying an Improved ABTS radical cation decolorization assay, Free Radic. Biol. Med. 26 (1999) 1231–1237.
[27] I. Gülçin, Antioxidant activity of caffeic acid (3,4-dihydroxycinnamic acid), Toxicology 217 (2006) 213–220, doi:10.1016/j.tox.2005.09.011.
[28] I. Gülçin, V. Mshvildadze, A. Gepdiremen, R. Elias, Screening of antiradical and antioxidant activity of monodesmosides and crude extract from Leontice smirnowii tuber, Phytomedicine 13 (2006) 343–351, doi:10.1016/j.phymed.2005.03.009.
[29] K. Aksu, B. Özgeriş, P. Taslimi, A. Naderi, İ. Gülçin, S. Göksu, Antioxidant activity, acetylcholinesterase, and carbonic anhydrase inhibitory properties of novel ureas derived from phenethylamines, Arch. Pharm. Chem. Life Sci. 349 (2016) 1–11.
[30] H.S. Tohma, I. Gulçin, Antioxidant and radical scavenging activity of aerial parts and roots of Turkish liquorice (Glycyrrhiza glabra L.), Int. J. Food Prop. 13 (2010) 657–671.
[31] D. Chen, X. Zhou, X. Chen, L. Huang, X. Xi, C. Ma, M. Zhou, L. Wang, T. Chen, Evaluating the Bioactivity of a Novel Antimicrobial and Anticancer Peptide, Dermaseptin-PS4(Der-PS4), from the Skin Secretion of Phyllomedusa sauvagii, Molecules 24 (2019) 2974, doi:10.3390/molecules24162974.
[32] P. Kumar, M. Duhan, K. Kadyan, J. Sindhu, S. Kumar, H. Sharma, Synthesis of novel inhibitors of α-amylase based on the thiazolidine-4-one skeleton containing a pyrazole moiety and their configurational studies, Medchemcomm 8 (2017) 1468–1476, doi:10.1039/c7md00080d.
[33] Molinspiration cheminformatics, Choice Rev. Online. 43 (2006) 43–65 38-43–6538, doi:10.5860/CHOICE.43-6538.
[34] A. Daina, O. Michielin, V. Zoete, SwissADME: a free web tool to evaluate pharmacokinetics, drug-likeness and medicinal chemistry friendliness of small molecules, Sci. Rep. 7 (2017) 1–13, doi:10.1038/srep42717.
[35] Schrödinger Release 2021-1: MaestroSchrödinger, LLC, New York, NY, 2021.
[36] D. Isika, M. Çeşme, F.J. Osonga, O.A. Sadik, Novel quercetin and apigenin-acetamide derivatives: design, synthesis, characterization, biological evaluation and molecular docking studies, RSC Adv 10 (2020) 25046–25058, doi:10.1039/d0ra04559d.
[37] T. Settypalli, V.R. Chunduri, A.K. Maddineni, N. Begari, R. Allagadda, P. Kotha, A.R. Chippada, Design, synthesis,: in silico docking studies and biological evaluation of novel quinoxaline-hydrazide hydrazone-1,2,3-triazole hybrids as α-glucosidase inhibitors and antioxidants, 2019. https://doi.org/10.1039/c9nj02580d.
[38] A. Bistrović, L. Krstulović, A. Harej, P. Grbčić, M. Sedić, S. Koštrun, S.K. Pavelić, M. Bajić, S. Raić-Malić, Design, synthesis and biological evaluation of novel benzimidazole amidines as potent multi-target inhibitors for the treatment of non-small cell lung cancer, Eur. J. Med. Chem. 143 (2018) 1616–1634.
[39] X. Creary, A. Anderson, C. Brophy, F. Crowell, Z. Funk, Method for assigning structure of 1,2,3-triazoles, J. Org. Chem. 77 (2012) 8756–8761.
[40] M.M. Rammah, W. Gati, H. Mtiraoui, M.E.B. Rammah, K. Ciamala, M. Knorr, Y. Rousselin, M.M. Kubicki, Synthesis of isoxazole and 1,2,3-Triazole isoindole derivatives via Silver- and copper-catalyzed 1,3-Dipolar cycloaddition reaction, Molecules. 21 (2016) 307, doi:10.3390/molecules21030307.
[41] R. Elancheran, K. Saravanan, S. Divakar, S. Kumari, V.L. Maruthanila, S. Kabilan, M. Ramanathan, R. Devi, J. Kotoky, Design, synthesis and biological evaluation of Novel 1, 3- thiazolidine-2, 4-diones as Anti-prostate cancer agents, Anticancer. Agents Med. Chem. 17 (2018), doi:10.2174/1871521409666170412121820.
[42] V.L. Maruthanila, R. Elancheran, N.K. Roy, A. Bhattacharya, A.B. Kunnumakkara, S. Kabilan, J. Kotoky, In silico molecular modelling of selected natural ligands and their binding features with estrogen receptor alpha, Curr. Comput. Aided. Drug Des. 15 (2018) 89–96, doi:10.2174/1573409914666181008165356.
[43] H.G. Eichler, A. Korn, S. Gasic, W. Pirson, J. Businger, The effect of a new specific α-amylase inhibitor on post-prandial glucose and insulin excursions in normal subjects and Type 2 (non-insulin-dependent) diabetic patients, Diabetologia 26 (1984) 278–281, doi:10.1007/BF00283650.
[44] S.H. Yoon, J.F. Robyt, Study of the inhibition of four alpha amylases by acarbose and its 4 IV-α-maltohexaosyl and 4IV-α-maltododecaosyl analogues, Carbohydr. Res. 338 (2003) 1969–1980, doi:10.1016/S0008-6215(03)00293-3.
[45] R. Bashary, G.L. Khatik, Design, and facile synthesis of 1,3 diaryl-3-(arylamino)propan-1-one derivatives as the potential alpha-amylase inhibitors and antioxidants, Bioorg. Chem. 82 (2019) 156–162.
[46] C. S., S. D.K., V. Ragunathan, P. Tiwari, A. S., B.D. Brindha Devi, Molecular docking, validation, dynamics simulations, and pharmacokinetic prediction of natural compounds against the SARS-CoV-2 main-protease, J. Biomol. Struct. Dyn. (2020) 1–27, doi:10.1080/07391102.2020.1815584.
[47] N.N. Sepay, N.N. Sepay, A. Al Hoque, R. Mondal, U.C. Halder, M. Muddassir, In silico fight against novel coronavirus by finding chromone derivatives as inhibitor of coronavirus main proteases enzyme, Struct. Chem. 31 (2020) 1831–1840, doi:10.1007/s11224-020-01537-5.
[48] K.R. Raghi, D.R. Sherin, M.J. Saumya, P.S. Arun, V.N. Sobha, T.K. Manojkumar, Computational study of molecular electrostatic potential, docking and dynamics simulations of gallic acid derivatives as ABL inhibitors, Comput. Biol. Chem. 74 (2018) 239–246, doi:10.1016/j.compbiolchem.2018.04.001.
[49] U. Vanitha, R. Elancheran, V. Manikandan, S. Kabilan, K. Krishnasamy, Design, synthesis, characterization, molecular docking and computational studies of 3-phenyl-2-thioxoimidazolidin-4-one derivatives, J. Mol. Struct. 1246 (2021) 131212, doi:10.1016/j.molstruc.2021.131212.
[50] M. Hagar, H.A. Ahmed, G. Aljohani, O.A. Alhaddad, Investigation of some antiviral N-heterocycles as COVID 19 drug: molecular docking and DFT calculations, Int. J. Mol. Sci. 21 (2020), doi:10.3390/ijms21113922.